ELSEVIER

Intermetallics 9 (2001) 73–79

Intermetallics

www.elsevier.com/locate/intermet

Deformation of a multiphase Mo–9.4Si–13.8B alloy at elevated temperatures

T.G. Nieh [a,*], J.G. Wang [b], C.T. Liu [c]

[a] *Chemistry and Materials Science, Lawrence Livermore National Laboratory, Livermore, CA 94550, USA*
[b] *Department of Materials Science and Engineering, Pennsylvania State University, PA 92697, USA*
[c] *Metals and Ceramics Division, Oak Ridge National Laboratory, Oak Ridge, TN 37831, USA*

Received 17 May 2000; accepted 19 July 2000

Abstract

A 3-phase silicide alloy, Mo–9.4Si–13.8B (at.%), was prepared via powder metallurgy techniques. The tensile properties of the alloy at elevated temperatures were evaluated in vacuum at temperatures ranging from 1350 to 1550°C and strain rates ranging from 5.0×10^{-4} to 1×10^{-3} s^{-1}. The alloy was found to exhibit a stress exponent of about 2.8 and relatively a high activation energy 740 kJ/mol. Also, it displayed unusually large tensile ductility (>100%) at $T>1400$°C. The deformation mechanism as well as large ductility are discussed in the light of the microstructural observations. The alloy has a very good mechanical strength at elevated temperatures, comparable to some of the most advanced tungsten-based alloys. © 2001 Elsevier Science Ltd. All rights reserved.

Keywords: A. Molybdenum silicides; B. Mechanical properties at high temperatures; B. Superplastic behavior; D. Defects: dislocation geometry and arrangement

1. Introduction

Mo_5Si_3 is one of the intermetallic phases in the Mo–Si binary system with the highest melting point (2180°C), and has the largest homogeneity range (2.5 at.% Si). It possesses excellent creep resistance at high temperatures, primarily because the bonding in Mo_5Si_3 has pronounced covalent components [1]. Although the compound has a poor oxidation resistance [2], the oxidation properties of Mo_5Si_3 can be substantially improved by adding boron [3,4]. For example, the oxidation rate of Mo_5Si_3 was lowered by 5 orders of magnitude over a temperature range of 800–1500°C by doping with less than 1 wt.% boron [3]. In fact, the oxidation rate of a Mo_5Si_3-matrix material containing 1.6 wt.% boron has been demonstrated to be comparable to that of $MoSi_2$ oxidized at 1450°C under identical conditions [5]. Recently, considerable efforts have thus been devoted to the study of the Mo–Si–B system [6–8].

The phase diagram of the ternary system Mo–Si–B was first constructed by Nowotny et al. in 1957 [9], and was recently advanced by Perepezko and co-workers [7,10], and Huebsch et al. [11]. The Mo-rich end of the phase diagram contains a number of intermetallic phases, including Mo_3Si, Mo_5Si_3 (T1), Mo_5SiB_2 (T2), MoB, and Mo_2B, which are all brittle at ambient temperature. It is worth noting that the existence of the stable ternary compound, Mo_5SiB_2, creates a number of ternary phase fields, allowing the control of material property via microstructural manipulation. For example, Schneibel et al. [12,13] studied a silicide alloy Mo–26.7Si–7.3B (at.%) located in the T1–T2–Mo_3Si field and found that it was brittle even at 1200°C. Liu et al. [6] investigated several Mo–Si–B alloys and found that a multiphase Mo–9.4Si–13.8B alloy containing ductile Mo-rich particles has a fracture toughness and flexure strength distinctly higher than that of silicides (Mo_5Si_3 or $MoSi_2$) without ductile Mo particles. The Mo–9.4Si–13.8B alloy exhibits a respectable fracture toughness of 10 MPa $m^{1/2}$ and flexure strength of 570 MPa at room temperature. Comparing with $MoSi_2$ [14], the alloy is also tougher than $MoSi_2$ by a factor of 4. The purpose of the present paper is to characterize the high-temperature deformation behavior of the Mo–9.4Si–13.8B alloy. An understanding of the deformation behavior would provide guidelines for hot forming since silicides are known to be difficult for machining.

* Corresponding author. Tel.: +1-925-423-9802; fax: +1-925-423-8034.

E-mail address: nieh1@llnl.gov (T.G. Nieh).

0966-9795/01/$ - see front matter © 2001 Elsevier Science Ltd. All rights reserved.
PII: S0966-9795(00)00098-4

2. Experiments

The alloy Mo–9.4Si–13.8B used in the present study was prepared by a powder metallurgy technique (PM) using elemental powders. The PM processing was carried out by mixing elemental powders in argon and hot-pressing compacts in vacuum in a 60-mm diameter graphite die at 1650°C and 48 MPa. The alloy ingot was further homogenized at 1400°C for 150 h in vacuum (10^{-7} Pa). The alloy contained 1100 wppm oxygen and 600 wppm carbon, which resulted in the formation of SiO_2 and B_2O_3 glass particles; its microstructure and phase composition have been reported previously [6].

Tensile sheet specimens were fabricated from the annealed material by electrical discharge machining. Tensile tests were conducted with an Instron machine equipped with a high temperature furnace. Tensile tests were carried out in a vacuum (10^{-3} Pa) system. The tensile fixture, which was essentially a universal joint with a pin-loading mechanism for the test sample, was made of potassium-doped tungsten and was designed to minimize misalignment of the test system. The crosshead movement was monitored by a computer equipped with a data aquisition system that controls tests under either constant crosshead speed or constant true strain rate condition. Test temperatures ranging from 1350°C to 1550°C (the test temperature was controlled within ±5°C) and strain rates ranging from 5.0×10^{-4} to 1×10^{-3}/s were used.

The microstructure of the P/M alloy was examined using a JEOL-200CX transmission electron microscope. TEM samples were first sliced from the alloy, and then lapped and thinned using SiC papers. Final thinning and perforation of TEM foils were conducted by twin-jet electropolishing in a solution of 60% methanol, 35% butyl alcohol and 5% perchloric acid at ~15V and −30°C.

3. Results

3.1. Microstructure before deformation

The consolidated material was essentially fully dense without any visible porosity and microcrack under optical microscope. X-ray diffraction pattern and electron microprobe analyses indicate that three phases

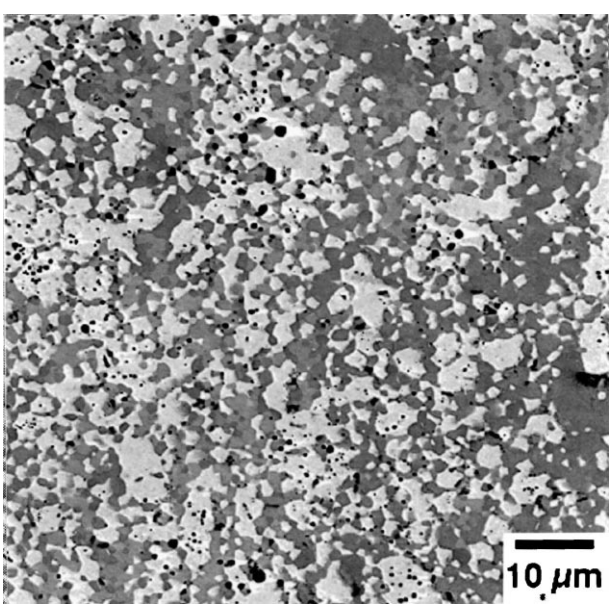

Fig. 1. Back-scattered electron image of the Mo–9.4Si–13.8B alloy showing a fine grain size (~3 μm), 3-phase microstructure. The light phase is the α-Mo solid solution.

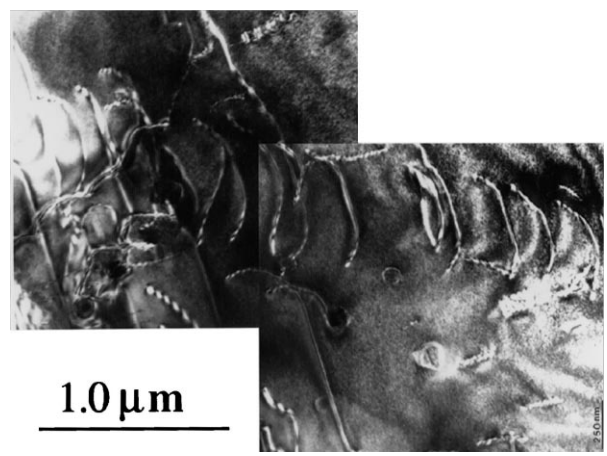

Fig. 2. Polygonal sub-grain structures observed in the Mo_3Si phase. Dislocations in the Mo_3Si phase were determined to be in the ⟨100⟩ direction.

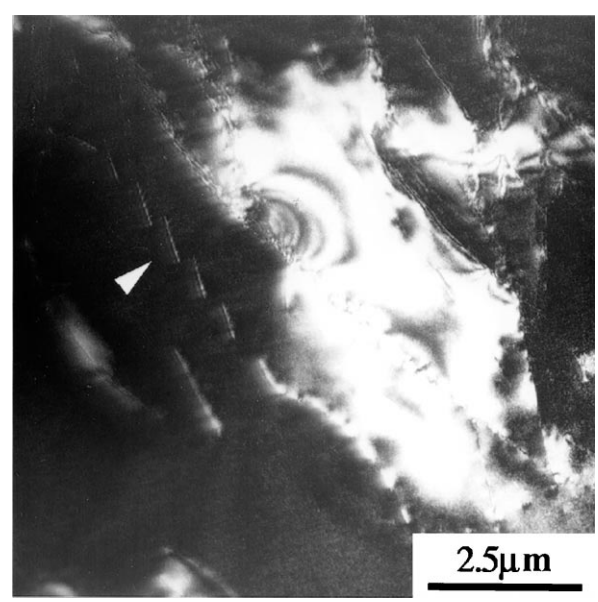

Fig. 3. Only few dislocations were observed in the T2 phase in the compressed sample.

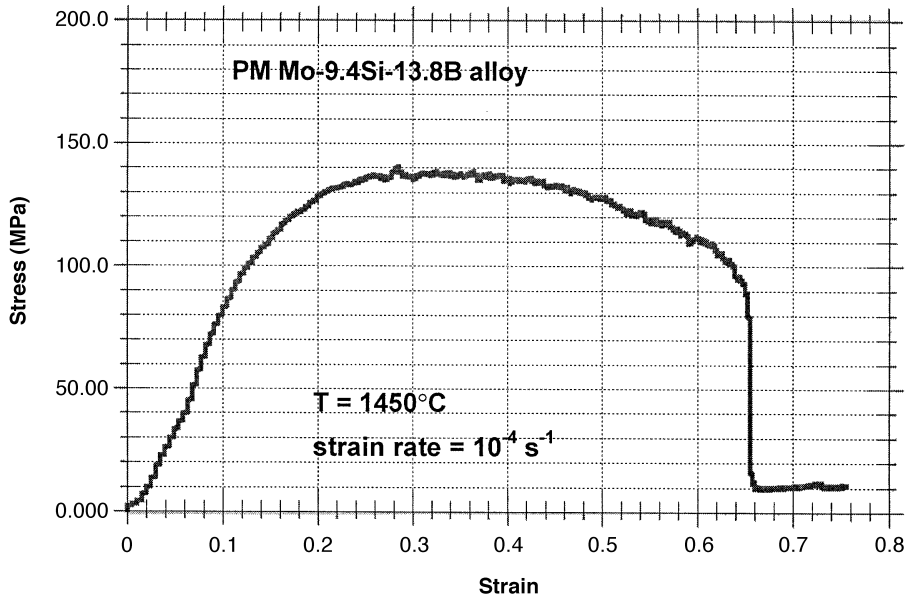

Fig. 4. Stress–strain curve of the Mo–9.4Si–13.8B alloy tested at a strain rate of 10^{-4}/s and 1450°C.

were included in the microstructure — Mo_5SiB_2 (T2 phase), Mo_3Si and an α-Mo solid solution. A back-scattered electron image of the alloy is given in Fig. 1. The alloy has a fine microstructure with an average grain size of about 3 μm for all phases. In Fig. 1, the light phase is the Mo-rich phase containing 1.5 at.% Si and 3.6% B, and the dark matrix phase is a mixture of two silicide phases with the compositions: Mo–21Si–7B [$Mo_3(Si,B)$] and Mo–11Si–34B [$Mo_5(Si,B)_3$]. The average microhardness value was measured to be 820 DPH, with 1160 DPH and 440 DPH for the silicide matrix and Mo-rich phases, respectively. The alloy contains 1100 wppm oxygen and 600 wppm carbon, resulting the formation of SiO_2 and borosilicate glass particles. In fact, some of the fine dark spots in Fig. 1 are glass particles. The volume fraction of the α-Mo is estimated to be about 50%.

The microstructures of both the as-annealed and mechanically deformed samples were examined using TEM. The deformed specimen was prepared by compressing a sample at 1400°C to a strain of about 10%. A high density of stacking faults was observed in the α-Mo phase, which appeared to be the softest. In both samples polygonal sub-grain structures were observed in the Mo_3Si phase (Fig. 2). Dislocation orientation in Mo_3Si phase was determined using a **g**·**b** method. In the two beam conditions, the dislocations are out of contrast using **g** = 002 and **g** = 022, but in contrast using **g** = 200. Thus, the Burgers vector of dislocation was determined to be ⟨100⟩. Whereas no dislocation was observed in the T2 phase in the annealed sample, very few dislocations were observed in the T2 phase in the compressed sample (Fig. 3), suggesting that T2 is the hardest among the three phase constituents. These dislocations have a line direction of ⟨100⟩, determined by **g**·**b** analysis. This indicates possibly the (001)⟨100⟩ basal slip; as observed by Meyer et al. [2].

3.2. Mechanical properties

The stress–strain rate curve of the Mo–9.4Si–13.8B alloy tested at 1450°C and a strain rate of 10^{-4} s^{-1} is shown in Fig. 4. The flow stress exhibits an initial strain hardening, reaching a peak, and followed by a gradual softening and sudden rupture. Typically, the flow stress peaks at the deformation strain of about 0.2. The initial hardening rate depends upon the applied strain rate and test temperature. In general, a faster strain rate or lower temperature favors a higher strain hardening rate. It is also observed in Fig. 4 that the alloy is readily deformed at high temperatures. In fact, a tensile elongation of 150% was measured from the sample tested at 1400°C and a strain rate of 10^{-4}/s. The tensile ductility decreased rapidly with decreasing temperature and increasing strain rate. For instance, at 10^{-4}/s and a

Table 1
Tensile peak stress and elongation at different strain rates and temperatures for Mo–9.4Si–13.8B alloy

Temperature	Peak stress (MPa)/tensile elongation (%) at different strain rates			
	10^{-4}/s	5×10^{-4}/s	10^{-3}/s	5×10^{-3}/s
1350°C	450/25	–	–	–
1400°C	222/150	415/27	480/23	–
1450°C	138/88	280/47	275/35	550/15
1550°C	–	–	175/62	–

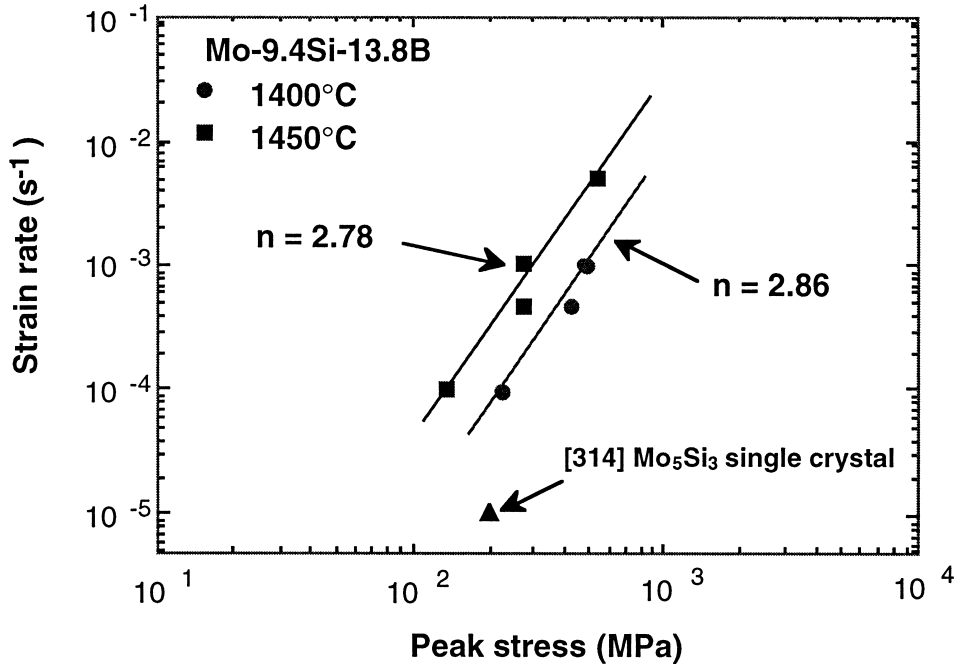

Fig. 5. Strain rate as a function of the peak stress for the Mo–9.4Si–13.8B alloy at 1400 and 1450°C.

temperature of 1350°C, the tensile ductility was only 25%. Also, at a higher strain rate of 10^{-3}/s, the alloy exhibited only a 20% tensile elongation at 1400°C. A summary of the peak stresses and tensile elongations of the Mo–9.4Si–13.8B alloy at different strain rates and temperatures is listed in Table 1.

To characterize the plastic flow behavior, the strain rate as a function of the peak stress for the Mo–9.4Si–13.8B alloy at 1400 and 1450°C is plotted in Fig. 5. The 1400°C strength of a [314] single-crystal Mo_5Si_3 reported by Mason [15] is also included in Fig. 5 for comparison. The single-crystal Mo_5Si_3, even in the [314] soft orientation, is stronger than the present multiphase Mo-Si-B alloy. As shown in Fig. 5, the stress exponent for the present alloy is calculated to be about 2.8. It is noted that Meyer et al. [15] also studied the creep properties of a powder-metallurgy Mo_5Si_3 alloyed with 13 wt.% B at temperatures ranging from 1240 to 1320°C and stresses ranging from 120 to 180 MPa. The alloy, having an average grain size of about 4 μm, was also 3-phase, consisting of Mo_5Si_3 (T1), Mo_3Si, and a ternary $Mo_5(Si,B)_3$ (T2). Whereas the average creep stress exponent was determined to be $n = 4.3$, there was a general trend that the n value decreased with increasing testing temperature. Specifically, the n value was 5.0 at 1242°C but reduced to 3.7 at 1302°C [2]. These testing temperatures are lower than those used in the present study (> 1350°C).

The relatively low n value of 2.8 obtained in the present study is expected to give rise to large plasticity. In fact, this expectation is consistent with the observations, as graphically shown in Fig. 6. The absence of necking can also be deduced from the abrupt drop in flow stress in the final stage of deformation (Fig. 4).

3.3. Activation energy

As shown in Fig. 7, the activation energy for deformation, assuming a mean n value of 2.8, is calculated to be 740 kJ/mol. This is much higher than the 396 kJ/mol obtained from compressive creep of the 3-phase Mo_5Si_3–13 wt.% B alloy [2].

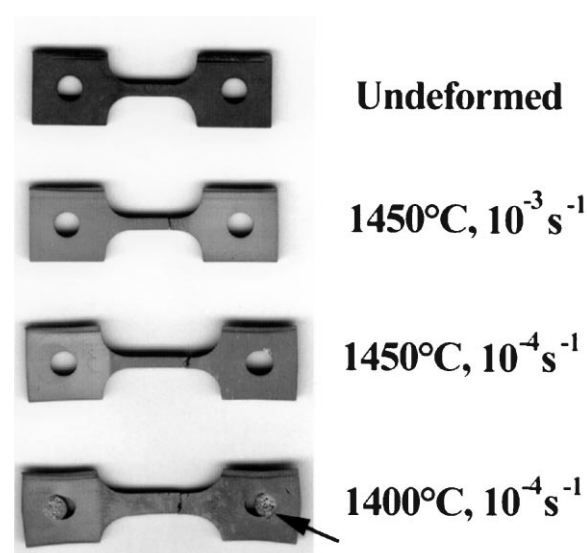

Fig. 6. Macroscopic view of the tested samples showing limited necking in all samples.

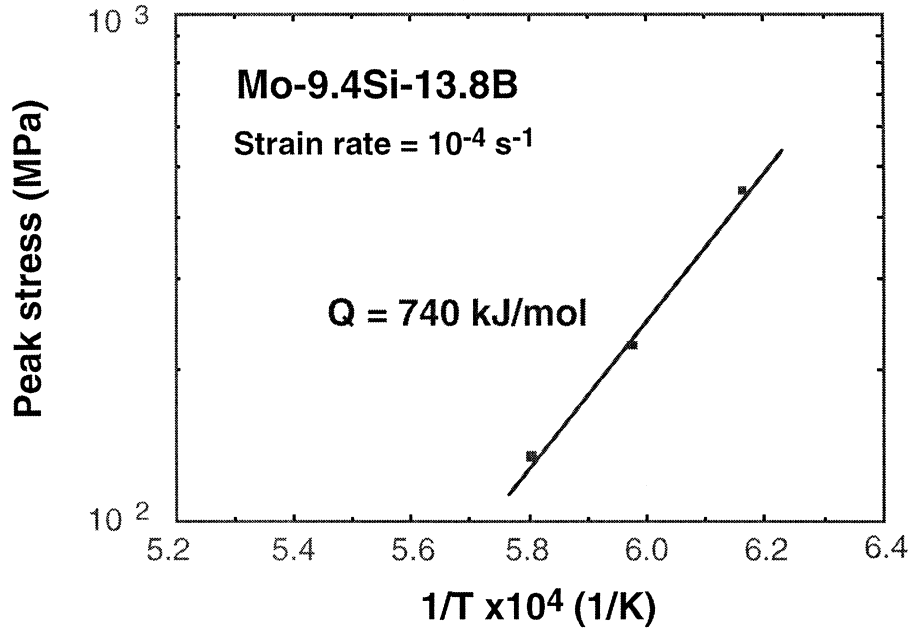

Fig. 7. Activation energy for deformation, assuming a mean n value of 2.8, is calculated to be 740 kJ/mol.

A high activation energy has often been attributed to the existence of threshold stresses. However, there is no indication of the existence of a threshold stress in the present data (Fig. 5). Therefore, the physical meaning of the high activation energy is unclear, especially since the alloy contains a soft α-Mo phase. Nonetheless, high activation energy normally indicates great difficulty for deformation.

3.4. Fracture surface

The fracture surface of a sample tested at 1450°C and a strain rate of 10^{-4}/s is depicted in Fig. 8. After deforming to a large plastic strain (~0.8), the fine-grained (~3.5 μm) microstructure was still retained, illustrating its high thermal stability. Grains are generally round and smooth as a result of extensive surface diffusion at high temperatures. Fracture surface exhibits an intergranular fracture mode without revealing any ductile dimple. These observations suggest that the large plasticity is primarily a result of intergranular sliding caused by the fine grains, not a result of intragranular deformation.

4. Discussion

From mechanical deformation point of view, the microstructure of the present alloy has two special features-fine grain size (3 μm), and a considerable amount of α-Mo solid solution (50% volume fraction). For a fine-grained alloy, grain/interface boundary sliding process normally dominates at the high testing temperatures (> 1350°C). However, as discussed early, α-Mo is soft and readily deformable at these testing temperatures. In comparison, the other two phases, Mo_3Si and T2, are much less deformable. Since the alloy consists of a high volume fraction of α-Mo phase, plastic straining from the -Mo phase is expected to contribute significantly to the total deformation. Therefore, plasticity of the alloy is a summation of two deformation processes: boundary sliding and bulk deformation of soft α-Mo.

It is known that the creep of Mo follows a 5th power law, i.e. $\dot{\varepsilon} = A_{Mo}\sigma^5$, where $\dot{\varepsilon}$ is the strain rate, and σ the flow stress [16]. The constitutive law for grain boundary sliding, on the other hand, can be generally described by $\dot{\varepsilon} = A_{gbs}\sigma^2$. Therefore, the total plastic strain rate, $\dot{\varepsilon}_{total}$, can be written as:

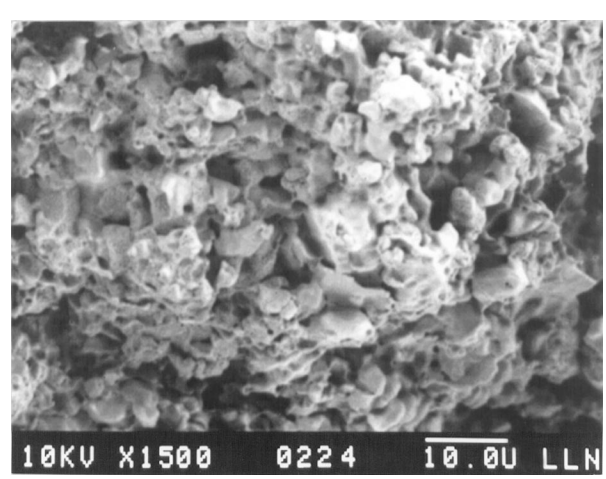

Fig. 8. Fracture surface of a sample tested at 1450°C and a strain rate of 10^{-4}/s.

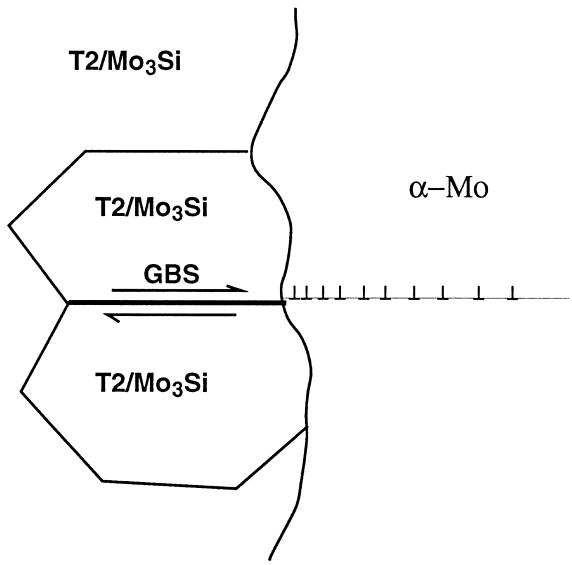

Fig. 9. Schematic illustration of strain accommodation at grain triple junctions by soft α-Mo.

$$\dot{\varepsilon}_{\text{total}} = A_{\text{gbs}}\sigma^2 + A_{\text{Mo}}\sigma^5 \quad (1)$$

It is evident from Eq. (1) that the stress exponent would fall between 2 and 5; this appears to be consistent with the experimentally observed n value of about 2.8 obtained in the present study.

The present silicide alloy is particularly noted to exhibit unusually large tensile ductility. This is attributed to the fact that it contains a continuous α-Mo network. It is generally recognized that grain boundary sliding (GBS) is the principal deformation mode in fine-grained alloys at high temperatures. During grain boundary sliding, the sliding strain must be properly accommodated by dislocation slip across neighboring grains. Otherwise, high local stresses at grain triple points are expected to be developed and lead to cavitation failure. Slip accommodation involves the sequential steps of glide and climb, with the slower of the two processes being rate-controlling. In the present silicide alloy, the microstructure consists of fine T2, Mo_3Si, and ~50% α-Mo phases. Strain accommodation at grain triple junctions can be readily achieved by the emission of dislocations into α-Mo grains, as schematically illustrated in Fig. 9. Since dislocation slip (either climb or glide) is easier in α-Mo grains than in either T2 or Mo_3Si grains, the presence of the soft α-Mo is obviously beneficial in reducing the stress at grain triple junctions and, thus, delaying cavitation and fracture. This offers an explanation for the large tensile elongation observed in the present Mo-matrix alloy. Thus, the soft α-Mo phase not only contributes directly to the total deformation via bulk deformation, but also plays a major role during boundary sliding. It is particularly pointed out that the above accommodation mechanism is not possible for silicide-matrix system because slip of silicide is difficult even at high temperatures. For instance, Meyer et al. [2] performed the compressive creep of a 3-phase, Mo_5Si_3 (T1), Mo_3Si, and $Mo_5(Si,B)_3$ (T2). Despite a fine grain size (4 μm) the compression strain was generally low (< 10%).

The high-temperature strength of the present Mo–9.4Si–13.8B silicide is quite remarkable. For example,

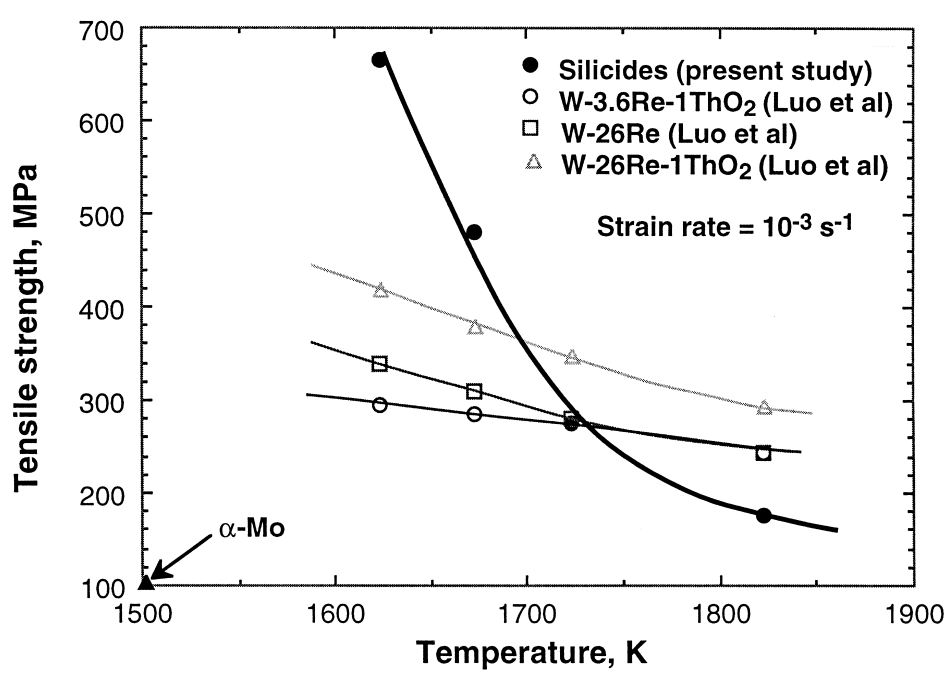

Fig. 10. The strength of the present Mo–9.4Si–13.8B silicide is comparable to that of some ultrahigh temperature tungsten alloys, e.g. W-Re-ThO_2 [19–21].

the tensile strength of unalloyed Mo (α-Mo) is about 100 MPa at 1200°C [16]. Even commercial TZM-Mo alloy at 1315°C exhibits a value of only 369 MPa [17]. In comparison, the present Mo-matrix alloy exhibits a tensile strength of 450 MPa at a higher temperature of 1350°C and relatively slow strain rate of 10^{-4}/s. The strengthening is obviously a result of the presence of strong silicide phases, Mo_3Si and Mo_5SiB_2; this is similar to that usually observed in ceramic particle reinforced metal matrix composites. It is also of interest to note that the present Mo–9.4Si–13.8B alloy is stronger than some advanced in situ Nb-based silicides [18]. These in situ silicides typically have yield strengths of 350 MPa at 1200°C, with creep rates of 10^{-8}/s at 1200°C and 100 MPa. The strength of the present silicide is comparable to that of some ultrahigh temperature tungsten alloys, e.g. W-Re-ThO_2 [19–21], as shown in Fig. 10. In fact, the present silicide is so strong that even K-doped tungsten pin used to load tensile specimens was broken during testing, as indicated (marked by arrow) in Fig. 6.

5. Conclusion

A Mo–9.4Si–13.8B alloy was produced by a powder metallurgy method. The alloy has a fine grain size (~3 μm) and is 3-phase, consisting of Mo_5SiB_2 (T2 phase), Mo_3Si, and 50 vol% α-Mo solid solution. Mechanical properties of the alloy at elevated temperatures (1350–1550°C) were evaluated in tension. The alloy exhibits a stress exponent of about 2.8 and activation energy 740 kJ/mol. Microstructural examination indicates that dislocation activity occurs primarily in α-Mo, with some limited activities in Mo_3Si, but virtually no activity in the T2 phase. The alloy exhibits a high strength of about 500 MPa at 1400°C and a strain rate of 10^{-3}/s; this is comparable to high-strength tungsten-based alloys. Despite the high strength, the alloy also shows extensive plasticity at temperatures above 1400°C. This is a result of the fact that the alloy contains a continuous α-Mo network. During grain boundary sliding, the soft α-Mo grains accommodate the sliding strain and reduce the propensity for cavitation at grain triple junctions and, thus, delay the fracture process.

Acknowledgements

This research was supported by the Division of Materials Sciences, Office of Basic Science, US Department of Energy under contract with Lawrence Livermore National Laboratory (contract No. W-7405-Eng-48) and UT-Battelle (contract no. DE-AC05-00OR22725).

References

[1] Fu CL, Wang XD, Ye YY, Ho KM. Intermetallics 1999;7(2):179.
[2] Meyer MK, Kramer MJ, Akinc M. Intermetallics 1996;4(4):273.
[3] Meyer MK, Akinc M. J Am Ceram Soc 1996;79(4):938.
[4] Meyer MK, Kramer MJ, Akinc M. Intermetallics 1999;7(2):153.
[5] Meyer MK, Akinc M. J Am Ceram Soc 1996;79(10):2763.
[6] Liu CT, Schneibel JH, Heatherly L. In: George EP, Yamaguchi M, Mills MJ, editors. MRS Proceeding on High-Temperature Ordered Intermetallic Alloys VII, Materials Research Society, Pittsburgh, PA, 1998: KK6.2.1.
[7] Sakidja R, Sieber H, Perepezko JH. Phil Mag Lett 1999;79(6):351.
[8] Akinc M, Meyer MK, Kramer MJ, Thom AJ, Huebsch JJ, Cook B. Mater Sci Eng 1999;A261(1–2):16.
[9] Nowotny H, Dimakopoulou E, Kudielka H. Monatsh Chem 1957;88:180.
[10] Nunes CA, Sakidja R, Perepezko JH. In: Nathal MV, editor. Structural intermetallics 1997, TMS, Warrendale, PA, 1997. p. 831.
[11] Huebsch JJ, Kramer MJ, Zhao HL, Akinc M. Intermetallics 2000;8:143.
[12] Schneibel JH, Liu CT, Heatherly L, Kramer MJ. Script Mater 1998;38(7):1169.
[13] Schneibel JH, Liu CT, Carmichael CA, Easton DS. Mater Sci Eng 1999;A261(1-2):78.
[14] Petrovic JJ. Mater Sci Eng 1995;A193:31.
[15] Mason DP, Van Aken DC. Acta Metall Mater 1995;43(3):1201.
[16] Metals ASF. Properties and selection: nonferrous alloys and special-purpose materials. 10th ed. Metals Park (OH): ASM International, 1990.
[17] Metals handbook. Properties and selection: stainless steels, tool materials and special-purpose materials. 9th ed. Metals Park (OH): ASM International, 1988.
[18] Bewlay BP, Jackson MR. In: Kelly A, Zweben C, Clyne TW, editors. Comprehensive composite materials, Vol 3, metal matrix composites. Elsevier, Oxford, in press.
[19] Luo A, Shin KS, Jacobson DL. Script Metall Mater 1991;25:2411.
[20] Luo A, Jacobson DL, Shin KS. Script Metall Mater 1991;25:1811.
[21] Luo A, Shin KS, Jacobson DL. Acta Metall Mater 1992;40(9):2225.